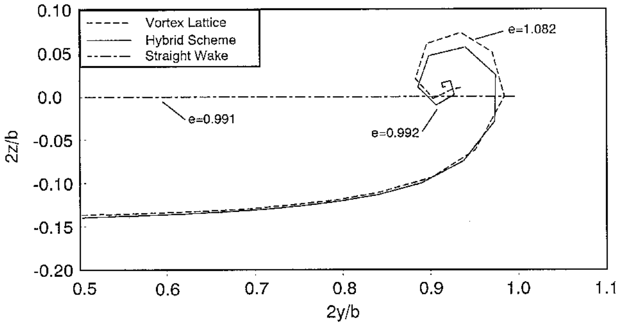

Fig. 3 Wake shapes produced by vortex-lattice and hybrid methods.

agreed within 0.1%, consistent with the hypothesis of Refs. 9 and 10. The agreement of the Trefftz-plane drag computed with the straight wake and the force-free wake, also 0.1%, indicates that the hybrid scheme produces force-free wakes of sufficient accuracy to enable Trefftz-plane integration of drag.

The hybrid method has also been successfully applied to an unusual split tip wing that has two outer wing panels in tandem, with no dihedral.[10] This planform is challenging for the wake-relaxation method because the wake from the forward tip panel passes closely over the rear tip panel. A conventional vortex-lattice method could not accommodate this close wake interaction because of the strong velocity singularities produced by the vortex elements on the wing. The drag prediction for the split tip wing using the hybrid wake method was in close agreement with high-resolution pressure integration as well as with wind-tunnel experiments using a wake survey method that enables direct measurement of induced drag.

Conclusions

A technique has been developed for numerically computing the force-free wake shape downstream of finite wings, based on the need for very accurate integration of induced drag in the Trefftz plane. An AR = 7 elliptical wing with straight trailing edge was used to study the influence of the computed wake shape on induced drag. A traditional vortex-lattice relaxation method produced a wake that led to a 9% error in Trefftz-plane drag. The new method presented here obtains more accurate wing-induced velocities from a high-order panel method, while relying on the well-behaved nature of the discrete-vortex wake model for the wake-induced velocities. The induced drag with the wake produced by this hybrid scheme agreed with the drag predicted with a straight wake within 0.1%, consistent with high-resolution pressure integration. These and other cited results indicate that the hybrid scheme produces wakes of sufficient accuracy to enable Trefftz-plane integration of drag on the force-free wake.

References

[1] Smith, S. C., and Kroo, I. M., "Computation of Induced Drag for Elliptical and Crescent-Shaped Wings," *Journal of Aircraft*, Vol. 30, No. 4, 1993, pp. 446-452.

[2] Dehaan, M. A., "Induced Drag of Wings with Highly Swept and Tapered Wing Tips," AIAA Paper 90-3062, Aug. 1990.

[3] Letcher, J. S., Jr., "Convergence of Lift and Drag Predictions by a Morino Panel Method (VSAERO)," *AIAA Journal*, Vol. 27, No. 8, 1989, pp. 1019, 1020.

[4] Carmichael, R. L., and Erickson, L. L., "PANAIR—A Higher Order Panel Code for Predicting Subsonic or Supersonic Linear Potential Flows About Arbitrary Configurations," AIAA Paper 81-1255, June 1981.

[5] Mittelman, Z., "Prediction of Unsteady Aerodynamics and Control of Delta Wings with Tangential Leading Edge Blowing," Ph.D. Dissertation, Stanford Univ., SUDDAR-580, Stanford, CA, June 1989.

[6] Quackenbush, T. R., Bliss, D. B., Wachspress, D. A., and Ong, C. C., "Free Wake Analysis of Hover Performance Using a New Influence Coefficient Method," NASA CR 4309, July 1990.

[7] Ashby, D. L., Dudley, M. R., and Iguchi, S. K., "Development and Validation of an Advanced Low-Order Panel Method," NASA TM 101024, Oct. 1988.

[8] Nagati, M. G., Iverson, J. D., and Vogel, J. M., "Vortex Sheet Modeling with Curved Higher-Order Panels," *Journal of Aircraft*, Vol. 24, No. 11, 1987, pp. 776-781.

[9] Kroo, I. M., and Smith, S. C., "Computation of Induced Drag with Nonplanar and Deformed Wakes," Society of Automotive Engineers Transactions, Paper 901933, Sept. 1990.

[10] Smith, S. C., "A Computational and Experimental Study of Nonlinear Aspects of Induced Drag," NASA TP 3598, Feb. 1996.

New Blunt Trailing-Edge Airfoil Design by Inverse Optimization Method

Shigeru Obayashi* and Shinkyu Jeong†
Tohoku University, Sendai 980-77, Japan
and
Yuichi Matsuo‡
National Aerospace Laboratory, Chofu 182, Japan

Introduction

AERODYNAMIC shape optimization is one of the major targets of computational fluid dynamics (CFD) today to improve design efficiency. Among aircraft components, optimization of airfoil shape has a significant impact on aircraft performance. Thus, transonic airfoil optimization is considered here.

In Ref. 1, a genetic algorithm (GA) has been applied to optimize target pressure distributions for inverse design methods. Pressure distributions around airfoils are parameterized by B-spline polygons, and the airfoil drag is minimized under constraints on lift, airfoil thickness, and other design principles. Once a target pressure distribution is obtained, corresponding airfoil geometry can be computed by an inverse design code coupled with a Navier-Stokes solver. Successful design results were obtained for transonic cases with and without a shock wave. In Ref. 1, a sharp trailing edge was employed for airfoil closure.

Traditionally, airfoil closure has been accomplished by using a sharp trailing edge. Work to develop the supercritical airfoil has shown the possibility of using a thin trailing-edge geometry with near-parallel trailing-edge surfaces to produce a superior transonic airfoil section. Further study by Henne[2] leads to a divergent trailing-edge airfoil that utilizes the bluntness of the trailing edge to improve transonic performance. Flowfields around such blunt trailing-edge airfoils have been studied numerically in Refs. 3-5.

In Ref. 6, the inverse optimization method was extended to the design of blunt trailing-edge airfoils. To predict the flowfield around the blunt trailing edge accurately, a grid was placed in the wake region behind the blunt trailing edge (the *H* grid) in addition to a grid wrapping around the airfoil sur-

Received Aug. 28, 1996; revision received Nov. 12, 1996; accepted for publication Nov. 18, 1996. Copyright © 1996 by the American Institute of Aeronautics and Astronautics, Inc. All rights reserved.

*Associate Professor, Department of Aeronautics and Space Engineering. E-mail: obayashi@ad.mech.tohoku.ac.jp. Senior Member AIAA.

†Graduate Student, Department of Aeronautics and Space Engineering.

‡Senior Scientist, Computational Sciences Division. Member AIAA.

face and the wake region (the C grid). Furthermore, the low Reynolds number k-ε model was implemented into the Navier–Stokes code to account for a separated flow at the base region as suggested in Ref. 4. Although the basic algorithm has been established, the quality of the result depends on the convergence of the inverse solver. This Note reports a new airfoil design obtained from an improved inverse solver.

Inverse Optimization Using GA

GAs simulate evolution by selection. Design candidates are considered as individuals in the population. An individual is characterized by genes represented as a string of parameters. In this Note, a B-spline curve is used to represent a pressure distribution. Seven points are used to define B-spline polygons to determine pressure distribution for the upper and lower airfoil surfaces separately. Except for the leading- and trailing-edge points, a total of 12 points are considered as genes representing design candidates.

At each generation (iteration) of GA, the fitness value (object function value) of every individual is evaluated and used to specify its probability of reproduction. A new population is generated from selected parents by performing crossover and mutation. Crossover proceeds in two steps. First, members in the mating pool are mated at random. Second, each pair of strings undergoes partial exchange of their strings at a random crossing site. This results in a pair of strings of a new generation. Mutation will occur during the crossover process at a given mutation rate. Mutation implies a random walk through the string space and it plays a secondary role. The present GA was run for 2000 generations with 100 individuals with a mutation rate of 20%.

In this Note, the optimization problem is defined as

Minimize: C_d
Subject to: 1. C_l = specified
2. Airfoil thickness t/c = specified

Reference 1 describes additional constraints based on the design principles of the supercritical airfoil. Those constraints are also necessary for the present optimization. Minor modifications were made to them here. For example, the maximum pressure coefficient at the rear loading region was increased to 0.5 to take advantage of the blunt trailing edge. The slope value of dC_p/dx to find a feasible location for a shock wave was reduced to 0.4 to produce a rooftop pressure distribution on the upper surface of the airfoil. Finally, the objective and constraints were combined into a single fitness function for the present GA (see Ref. 1 for details).

Once the present GA finds an optimum target pressure distribution, a corresponding airfoil geometry can be obtained by an inverse design method. Here, the inverse design code, WinDes, is used.[7] WinDes uses the following iterative procedure. Suppose an initial geometry and surface pressure distribution obtained from any CFD code is given. First, pressure differences are calculated from the given initial and target pressure distributions. From these pressure differences, corresponding geometry corrections can be computed from the integral equations discretized at the panels on the geometry. An improved geometry is then obtained from the initial geometry and the computed geometry corrections. Finally, the CFD code is used again to check how close the resulting pressure distribution is to the target distribution. If the differences are still large, the process is iterated. In practice, 15 design cycles are sufficient to obtain the final geometry.

The input for the inverse design code is pressure differences and the output is geometry corrections. To avoid reversed geometry definition at the trailing edge, the geometry correction is always set to zero at the trailing edge. If an initial airfoil has a blunt trailing edge, a designed airfoil should retain it. Thus, by using a shortened NACA 0012 with base as an initial airfoil, a blunt trailing-edge airfoil can be designed by WinDes. The base size was set to 0.7% chord.[8] When a strong shock wave appears, however, WinDes sometimes has difficulty in convergence of the design cycle. In the present study, convergence was achieved by applying smoothing to the modified geometry at each inverse design cycle.

The advantage of the present inverse method is that the required analysis code is arbitrary and any type of analysis method, even experiment, can be used. In this Note, the Navier–Stokes code validated in Ref. 6 was coupled together. In Ref. 6, numerical results of transonic flows around the shortened RAE2822 airfoil were compared with experiment similar to Refs. 3 and 4. For the present computation, the C grid of 191 × 91 points and the H grid of 32 × 32 points were used. The inverse design code, Navier–Stokes code, and algebraic grid generator constructs a nearly automated loop for the inverse design with reasonable computational requirements. These codes were implemented on a Cray C90 supercomputer at the Institute of Fluid Science, Tohoku University. The inverse design for 10 cycles required about 2 h of single CPU time.

Design Result

As a reference airfoil to be compared with a new design, NASA SC(2)-0714 was selected from Ref. 7. This airfoil is 14% chord thick. The design point of the airfoil is $C_l = 0.70$, $M = 0.73$, $Re = 30 \times 10^6$, and $\alpha = -0.06$ deg. The Navier–Stokes code used predicted $C_l = 0.806$ at the flow condition of $M = 0.73$, $Re = 30 \times 10^6$, and $\alpha = 0$ deg. These latter values were chosen as the present design point.

Figure 1 shows the comparison of computed pressure distribution of the designed airfoil against the target distribution. The target pressure distribution was optimized by GA. The corresponding geometry was obtained by the inverse design. The resulting pressure distribution was computed by the Navier–Stokes code. The aerodynamic performance of the designed airfoil becomes $C_l = 0.795$ and $C_d = 0.0136$ at the design point. Figure 2 shows a comparison of geometries between the designed and SC(2)-0714 airfoils.

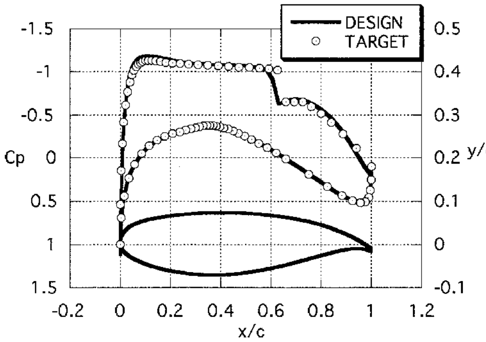

Fig. 1 Design result.

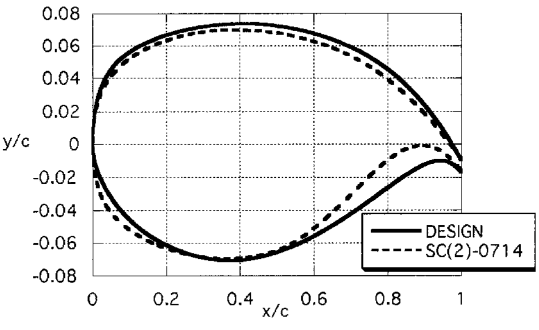

Fig. 2 Comparison of airfoil geometries.

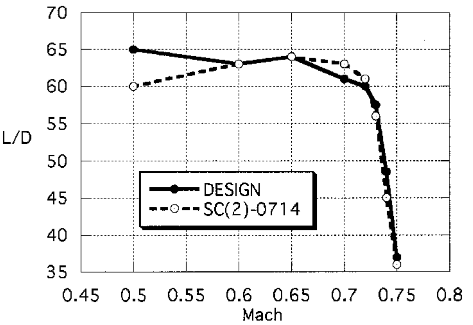

Fig. 3 Comparison of aerodynamic performance.

To compare relative aerodynamic performance, *L/D* is plotted at various Mach numbers in Fig. 3. From the plots, the present design is found to perform better than SC(2)-0714, except at Mach numbers of 0.7 and 0.72 (slightly lower than the design point of 0.73). Although only a straight base is considered for the airfoil closure here, Ref. 8 suggests that the inclusion of cavity at the base might further reduce the drag.

References

[1]Obayashi, S., and Takanashi, S., "Genetic Optimization of Target Pressure Distributions for Inverse Design Methods," *AIAA Journal*, Vol. 34, No. 5, 1996, pp. 881–886.

[2]Henne, P. A., "Innovation with Computational Aerodynamics: The Divergent Trailing-Edge Airfoil," *Applied Computational Aerodynamics*, edited by P. A. Henne, Vol. 125, Progress in Astronautics and Aeronautics, AIAA, Washington, DC, 1990, pp. 221–262.

[3]Stanaway, S. K., McCroskey, W. J., and Kroo, I. M., "Navier-Stokes Analysis of Blunt Trailing Edge Airfoils," AIAA Paper 92-0024, Jan. 1992.

[4]Monsen, E., and Rudnik, R., "Investigation of the Blunt Trailing Edge Problem for Supercritical Airfoils," AIAA Paper 95-0089, Jan. 1995.

[5]Thompson, B. E., and Lotz, R. D., "Divergent-Trailing-Edge Airfoil Flow," *Journal of Aircraft*, Vol. 33, No. 5, 1996, pp. 950–955.

[6]Obayashi, S., Jeong, S., and Matsuo, Y., "Inverse Optimization Method for Blunt-Trailing-Edge Airfoils," *Proceedings of the 15th International Conference on Numerical Methods in Fluid Dynamics* (Monterey, CA), Springer–Verlag, Berlin, 1997, pp. 206–211.

[7]Takanashi, S., "Iterative Three-Dimensional Transonic Wing Design Using Integral Equations," *Journal of Aircraft*, Vol. 22, No. 8, 1985, pp. 655–660.

[8]Harris, C. D., "NASA Supercritical Airfoils—A Matrix of Family-Related Airfoils," NASA TP-2969, March 1990.

Induced Drag Calculation by Numerical Lifting Surface Method

Masami Ichikawa* and Akira Matsuda*
Okayama Prefectural University,
Soja, Okayama 719-11, Japan

Nomenclature

b = wingspan length
C_{Di} = total induced drag coefficient
C_L = total lift coefficient
C_T = total thrust coefficient
c = local chord length
c_{di} = sectional induced drag coefficient
c_l = sectional lift coefficient
c_t = sectional thrust coefficient
S = wing planform area
T_n = Chebychev polynomial of degree n of the first kind
α = angle of attack
ΔC_p = difference between lower and upper pressure coefficients

Superscripts
F = far-field method
N = near-field method

Introduction

THE calculation of induced drag is one of the difficult problems for the discrete numerical lifting surface methods because it requires a very accurate computation of the lift distribution. Since the numerical accuracy near the leading edge of the conventional vortex lattice method (VLM) is not adequate, VLM cannot predict the near-field induced drag as precisely as that of the far field. There are several works[1,2] to improve the accuracy near the leading edge of the VLM solution. The quasi-vortex-lattice method (QVLM) by Lan[3] appears to be the only one among those methods that has succeeded in obtaining adequate results for two calculation methods of the induced drag. Most of the numerical lifting surface methods including QVLM have only investigated the agreement of the near- and far-field induced drags because it has been taken as the performance indicator of the numerical methods, but they have not addressed the accuracy of the predicted values sufficiently. In Ref. 4, the present authors have shown the analytical solutions of the induced drag in terms of the near and far fields for the elliptic wing in steady incompressible flow using Kida's method.[5] This Note investigates, through the analytical results in Ref. 4, the performance for the induced drag calculation of QVLM and box-in-strip method (BISM)[6] developed by one of the present authors.

Method

The computational method of the induced drag by QVLM is addressed in Ref. 3, whereas that by BISM must be formulated and incorporated into a computer program. First, the near-field induced drag calculation is considered.

Since BISM utilizes the Stark's quadrature formula[7] for evaluating the Cauchy singularity in the lifting surface integral equation, it calculates the values of ΔC_p at the points (x_i, y) expressed by the cosine law distribution:

$$x_i = x_m + (c/2)\cos\beta_i, \qquad i = 1, \ldots, n \tag{1}$$

where x_m denotes the x coordinate of the midpoint on the local chord, $\beta_i = 2i\pi/(2n + 1)$, and n is the total number of chordwise collocation points. The spanwise coordinate y of the collocation point can be determined arbitrarily and will not be specified here. It is found that cos β_i are the zero points of function $G_n(\xi)$ defined by $[T_{n+1}(\xi) - T_n(\xi)]/(1 - \xi)$, and it is also shown that $G_n(\xi)$ is the orthogonal polynomial of degree n on the interval $[-1, 1]$ with respect to the weighting function $[(1 - \xi)/(1 + \xi)]^{1/2}$, which expresses the singularity at the leading and trailing edges in the thin wing theory. Using the Lagrangian interpolation formula, the chordwise distribution of ΔC_p can be approximated by the following equation:

$$\Delta C_p(x, y) = \sum_{i=1}^{n} g_i(\xi)\Delta C_p(x_i, y) \tag{2}$$

Received Aug. 13, 1996; revision received Nov. 15, 1996; accepted for publication Nov. 30, 1996. Copyright © 1997 by the American Institute of Aeronautics and Astronautics, Inc. All rights reserved.

*Assistant Professor, Department of System Engineering, Faculty of Computer Science and System Engineering, Kuboki 111.